EFFECTS OF BOLT-HOLE CONTACT ON BEARING-BYPASS DAMAGE-ONSET STRENGTH

John H. Crews, Jr. and Rajiv A. Naik[1]

NASA Langley Research Center
Hampton, Virginia

ABSTRACT

A combined experimental and analytical study was conducted to investigate the effects of bolt-hole contact on the bearing-bypass strength of a graphite/epoxy laminate. Tests were conducted on specimens consisting of 16-ply quasi-isotropic T300/5208 laminates with a centrally located hole. Bearing loads were applied through a clearance-fit steel bolt. Damage-onset strength and damage mode were determined for each test case. A finite element procedure was used to calculate the bolt-hole stresses and bolt contact for each measured damage-onset strength.

For the tension bearing-bypass cases tested, the bolt contact half-angle was approximately 60° at damage onset. For compression, the contact angle decreased by 20° as the bypass load increased. A corresponding decrease in the bearing-damage onset strength was attributed to the decrease in contact angle which made the bearing loads more severe.

Hole boundary stresses were also computed by superimposing stresses for separate bearing and bypass loading. Stresses at the specimen net section were accurately approximated by the superposition procedure. However, the peak bearing stresses had large errors because the bolt contact angles were not represented correctly. For compression, peak bearing stress errors of nearly 50 percent were calculated.

INTRODUCTION

A fastener hole in a structural joint is typically subjected to a combination of bearing loading that is reacted at the hole and bypass loading that is reacted elsewhere. To predict the strength of composite joints, both types of loading must be accounted for. Unfortunately, the effects of the bearing and bypass loads are often coupled, causing load-interaction effects that can complicate the prediction of bearing-bypass strength. For tension bearing-bypass loading, the load-interaction effects are essentially a linear combination of the bearing and bypass effects and are rather easily predicted [1]. However, for compression, these load-interaction effects are not as well understood. Stress analyses and strength predictions for compression bearing-bypass loading are especially complicated when bolt-hole clearance is accounted for. For such cases the bolt-hole contact varies nonlinearly with loading and is difficult to calculate [2].

The present paper has two objectives. First, it will analyze the influence of bolt-hole contact on the bearing-bypass damage-onset strength of a composite laminate. Second, this paper will examine the need to account for varying bolt-hole contact when using stress analysis procedures based on the superposition of separate bearing and bypass analyses. This paper focuses on recent NASA Langley research on single-fastener specimens loaded with a range of bearing-bypass ratios [2-4]. Specimens were made with T300/5208 graphite/epoxy laminates having a 16-ply quasi-isotropic layup. Bearing loads were applied through a steel bolt at the center of the specimen. A NASA Langley developed test apparatus [2] was used to apply

---

1 Analytical Services and Materials, Inc., Hampton, Virginia

different ratios of bearing to bypass loading in tension as well as compression. Specimens were loaded until damage was detected and this was used as the damage-onset strength. A finite element analysis was then used to calculate the bolt-hole contact arc and the hole boundary stresses corresponding to each measured damage-onset strength. An inverse technique [5] was used to study the nonlinear bolt-hole contact using linear analysis methods.

First, the damage-onset strengths are presented and discussed. Then, the computed hole-boundary stresses and contact angles are presented and used to interpret the observed strength trends and load interactions. Finally, stress analysis results for simultaneous bearing and bypass loading are compared with those calculated by superposing bearing results and bypass results. Also, areas of future bearing-bypass research are briefly discussed.

LIST OF SYMBOLS

c	bolt-hole clearance, m
d	hole diameter, m
P_a	applied load, N
P_b	bearing load, N
P_p	bypass load, N
r_b	bolt radius, m
S_b	nominal bearing stress, MPa
S_{np}	nominal net-section bypass stress, MPa
t	specimen thickness, m
w	specimen width, m
x,y	Cartesian coordinates, m
θ_1	contact half-angle for single contact, deg
θ_2	contact half-angle for dual contact, deg
β	bearing-bypass stress ratio
$\sigma_{\theta\theta}$	tangential stress component, MPa
σ_{rr}	radial stress component, MPa

BEARING-BYPASS TESTING

Test Procedure

The test specimen configuration is shown in figure 1(a). The T300/5208 specimens were machined from a single $(0/45/90/-45)_{2s}$ panel. The bolt holes, machined using an ultrasonic diamond core drill, had a diameter d of 6.396 mm, which produced a clearance of 0.076 mm with the 6.320 mm steel bolts. This clearance was 1.2 percent of the hole diameter. The width-to-hole-diameter ratio (w/d) was 7.8.

The bearing-bypass loading notations for tension and compression are shown in figure 1(b). Test results are reported in terms of nominal gross-section stress S_g, nominal bearing stress S_b, and nominal net-section bypass stress S_{np}, calculated using the following equations:

$$S_g = P_a /tw$$

$$S_b = P_b / td$$

and

$$S_{np} = P_p / t (w - d)$$

The bearing-bypass ratio β was defined as

$$\beta = S_b / S_{np}$$

The test system used in this study is shown schematically in figure 2. This system uses two servo-controls. The center of the specimen is bolted between two bearing-reaction plates that are attached to the load frame using two load cells. The ends of the specimen are then gripped and loaded independently by the two servo-control systems (called Upper and Lower in figure 2). Any difference between these two end loads produces a bearing load at the central bolt hole. This bearing load is measured by the load cells under the bearing reaction plates. The end loads are synchronized by a common input signal; as a result, a constant bearing bypass ratio is maintained throughout each test.

The bearing reaction plates were bolted to the load cells allowing either tension or compression bearing loads. During compression, the bearing-reaction plates prevent specimen buckling. Hardened steel bushings were used between the bolt and the bearing-reaction plates. These 12.7 mm bushings were machined for a sliding fit, allowing the bolt clamp-up force to be transmitted to the local region around the bolt hole. This arrangement was equivalent to having a clamp-up washer directly against the surface of the specimen. For the present tests, the bolt was finger tightened (about 0.2 Nm torque) to produce a very small clamp-up force against the specimen.

Throughout each test, specimen deformation was measured by displacement transducers mounted symmetrically on the front and back of the bearing reaction plates. The transducer rods rested on small bars that were cemented to the specimen slightly above the grip line. This arrangement provided a measurement of the relative displacement between the bearing-reaction plates and the specimen. As explained in the following, these measurements were used to determine the damage onset.

For each test, the nominal bearing and bypass loads were plotted against the specimen displacement. As the specimens were slowly loaded, these load-displacement curves gradually became nonlinear. This nonlinearity was used to indicate damage initiation at the bolt hole. The intersection of each curve with a straight line offset by 0.001d was arbitrarily selected to define the damage-onset level. Specimens were unloaded after damage onset was indicated and were treated with an X-ray opaque dye-penetrant before being radiographed to determine the damage-onset mode.

Test Results

The damage-onset modes are shown by the radiographs in figure 3. For tension dominated loading, the damage developed in the net-section tension (NT) mode, figure 3(a). The gray shadows show delaminations and the dark bands indicate ply splits. The tension-reacted bearing (TRB) and compression-reacted bearing (CRB) damage modes are similar and appear to be delamination dominated. The net-section compression (NC) mode involves rather discrete damage zones extending from the hole. This damage was caused by microbuckling in the 0° plies [6].

The measured S_b and S_{np} values corresponding to damage onset are plotted against one another in figure 4, as a so-called bearing-bypass diagram. Each symbol represents the average of three tests (also see Table 1). The tick marks indicate

the range of measured strengths, plotted along lines of constant β. The curves were fit through the data and provide a failure envelope for bearing-bypass damage onset.

The right side of figure 4 shows tension results for four β values (0, 1, 3, ∞). The symbol on the S_{np} axis represents all-bypass loading ($\beta = 0$) in tension. The NT next to symbols indicates the net-section tension damage mode. As expected, all test cases that resulted in NT damage can be represented by a straight line and, thus, show the linear interaction discussed in [1] and [2]. This linearity suggests that the local stress that governs NT damage onset is the sum of the local stresses due to bearing loading and bypass loading. A horizontal "bearing cutoff" line was drawn through the $\beta = \infty$ data point which is labeled TRB to indicate tension reacted bearing damage. The compression reacted bearing (CRB) damage-onset strength is slightly smaller than the TRB damage-onset strength. The CRB damage-onset strength varies with bypass stress and therefore cannot be represented by a simple horizontal cutoff line. The compressive bypass stress decreases the CRB onset strength by five percent for $\beta = -3$ and about 40 percent for $\beta = -1$. This interaction between bearing and bypass loads was caused by a decrease in the bolt-hole contact arc and will be discussed in the next section. For the all-bypass compressive loading ($\beta = -0$), net-section compression (NC) damage initiated at -422 MPa. This NC damage-onset strength was much larger than expected and suggested that dual bolt-hole contact developed, allowing load transfer across the hole. Such contact reduces the compressive stress concentration at the net section and thereby increases the specimen strength. This will also be discussed later in an analysis of bolt-hole contact.

STRESS ANALYSIS

In this section, first, the stress analysis procedures are briefly described. Next, stress distributions along the hole boundary are shown for each measured damage-onset strength. These stress distributions are then used in a discussion of the critical local stresses associated with each damage mode. Finally, the bolt contact angles are presented and used in a discussion of the measured strengths for each damage-onset mode.

Inverse Stress Analysis Procedure

The finite element model and procedures used in this study were evaluated in [3]. The finite element calculations were performed using the NASTRAN finite element code. The contact arc was represented using displacement constraints along a portion of the hole boundary. Within an assumed contact arc, nodes on the hole boundary were constrained to lie on a circular arc corresponding to the bolt radius (r_b). This procedure represented a rigid bolt having a frictionless interface with the hole. Two-dimensional elements were used to model the test specimen. Along the hole boundary, the elements subtended less than 1^0. As a result, the contact arc could be modeled very accurately.

Because a bolt clearance was used, the contact angle at the bolt-hole interface varied with bearing stress, as shown in figure 5. This nonlinear problem was reduced to a linear problem by using an inverse procedure [7] as follows. For simple bearing loading, a contact angle was assumed and the corresponding bearing load was calculated. The contact stress σ_{rr} at the last finite element node of the contact arc must be equal to zero, point B in figures 5 and 6(a). This requirement is satisfied only when the "correct" bearing stress is used with the assumed contact angle, thereby, providing a criterion for calculating the correct bearing stress. For each assumed contact angle, two finite element analyses were performed each with an arbitrarily selected bearing stress. The two corresponding nonzero values of σ_{rr}

at the end of the arc were then used to calculate the correct bearing stress for the assumed contact angle [8]. This inverse procedure was repeated for a range of contact angles to establish a relationship between contact angle and bearing stress, as shown, for example, in figure 5.

The inverse procedure was extended in [5] to include bypass as well as bearing loading. For each bearing-bypass ratio β, the combined bearing and bypass loading was expressed in terms of the bearing stress S_b and β. For a given β, the procedure was identical to that used for pure bearing [8]. The calculations were repeated to establish a relationship between contact angle and bearing-bypass loading for each β value in the test program.

The inverse procedure was further extended in [5] to analyze cases of compression bearing-bypass loading that produced dual contact between the bolt and hole, as shown in figure 6(b). Such dual contact can develop when compressive bypass stresses produce hole deformations that are comparable to the bolt-hole clearance. In contrast to the single contact case, the bearing-bypass ratio could not be assumed. However, as in the single contact case, the contact stress was required to be zero at the last node of both contact arcs, points B and E in figure 6(b). For dual contact cases, values for both contact angles were assumed and the required combination of bearing and bypass loading was calculated as follows. Three finite element runs were made each with an arbitrarily selected combination of bearing and bypass stress. The three sets of corresponding non-zero values of computed contact stresses for the ends of the two contact arcs were then used to calculate the correct bearing-bypass combination for the assumed contact angles. This inverse procedure was repeated to obtain the desired relationships between compressive bearing-bypass loading and dual contact for the clearance used in this study. Results will be shown in the next section.

Stress Results

Figure 7 shows the computed $\sigma_{\theta\theta}$ and σ_{rr} stresses plotted along the hole boundary. Because of symmetry, these stresses are shown only along one-half of the hole boundary, from $\theta = 0°$ to $180°$. The four sets of curves in figure 7 correspond to the measured stress levels for damage onset in the tension bearing-bypass tests. For $\beta = 0$, 1 and 3, the $\sigma_{\theta\theta}$ curves have peak values near the specimen net section ($\theta = 90°$), and are within about 7 percent of the average peak value of 870 MPa. All three of these cases developed damage in the NT mode; therefore, 870 MPa seems to be the critical $\sigma_{\theta\theta}$ value for NT damage onset. For the bearing critical $\beta = \infty$ case, the $\sigma_{\theta\theta}$ peak of about 690 MPa is well below the critical 870 MPa level for NT damage. The σ_{rr} peak for the $\beta = \infty$ case is about -760 MPa; this is the peak contact stress corresponding to TRB damage onset. As expected, the peak σ_{rr} values for the other two tension bearing-bypass cases ($\beta = 1$ and 3) are well below 760 MPa. Notice that the σ_{rr} curves indicate bolt-hole contact over only about 60°. Because of symmetry, this corresponds to a contact angle of 120° but the half-angle shown in the figure will be subsequently referred to simply as the contact angle.

Figure 8 plots the $\sigma_{\theta\theta}$ and σ_{rr} stresses along the hole boundary for the measured strengths corresponding to damage onset in the four compression test cases ($\beta = -0$, -1, -3, and $-\infty$). The $\sigma_{\theta\theta}$ and σ_{rr} curves for the CRB $\beta = -\infty$ case are generally similar to those for the TRB $\beta = \infty$ case shown previously in figure 7, but the $\sigma_{\theta\theta}$ peak of about 550 MPa is considerably lower than the 690 MPa peak for TRB and much lower than the critical 870 MPa level for NT damage. The σ_{rr} peak of -800

925

MPa for the $\beta = -\infty$ case is about five percent larger than the 760 MPa value for the $\beta = \infty$ case. The peak σ_{rr} stresses for the three CRB cases ($\beta = -\infty$, -3, and -1) in figure 8 have an average value of 807 MPa. The $\beta = -0$ (all-bypass) case in figure 8 has a $\sigma_{\theta\theta}$ peak of 940 MPa at $\theta = 90°$ which corresponds to NC damage onset. The corresponding σ_{rr} stress distributions for $\beta = -0$ indicate dual contact over about 20° at both $\theta = 0°$ and 180°.

Bolt-Hole Contact Results

The variation of contact angle θ_1 with bearing stress S_b is shown in figure 9 for the various β values used in this study. The two all-bearing cases labelled $\beta = \infty$ and $-\infty$ are noticeably different from each other, differing by about five degrees for the range of measured bearing damage-onset strengths. The $\beta = 1$ and 3 curves show larger contact angles while the $\beta = -1$ and -3 curves indicate smaller angles, compared to the all-bearing cases. For $S_b = 500$ MPa, contact angles could differ by as much as 40° depending on which β is used.

To further discuss bolt-hole contact, the computed contact angles in figure 9 are replotted in a different way in figure 10. The contact angles are plotted against bypass stress S_{np} for three S_b levels (300, 400, and 500 MPa) which are typical of the measured strengths. This figure can be used to discuss the separate effects of clearance and bypass stress on the contact angle. In the absence of clearance or bypass stress, contact would occur over about 82° [9]. Figure 10 shows that a 0.076-mm clearance reduces the θ_1 contact angles to about 50°-60° for $S_{np} = 0$. Increasing the tensile bypass stress increases the θ_1 contact angle while increasing the compressive bypass stress decreases it. For large compressive bypass stresses, the θ_1 curves are influenced by dual contact.

To put this θ_1 behavior in perspective for the present study, the combinations of measured bypass strength and computed contact angles are shown as solid symbols in figure 10. These symbols show that the contact angles were nearly constant at about 60° for all three tension bearing-bypass test cases. However, this nearly constant behavior is probably coincidental and, therefore, is not believed to be typical of other laminates and specimen configurations. For the compression test cases, the contact angle varied by more than 20° for the range of tests and had a minimum value of about 35°. Figure 10 shows that clearance and bypass stresses can combine to reduce the contact angle to values that are significantly smaller than the 90° (semi-circular) value often assumed in analyses. For example, contact was modeled by imposing zero radial displacements over a semicirclar hole boundary in [10] and [11] and by a cosine distribution of radial stress over a semicircle in [12]. The importance of correctly modelling contact will be discussed in the next section.

Recall that figure 4 showed that CRB damage-onset strength decreased with increasing levels of compressive bypass stress. When this interaction was first observed, it was unexpected because CRB damage is caused by the σ_{rr} contact stress and the compressive bypass loads were not expected to have much influence on σ_{rr}. This interaction for compression bypass loading can be explained using figure 10. As mentioned above, θ_1 decreased by about 20° as the bypass loads became more compressive. These smaller contact angles allowed smaller bearing loads to produce the same critical σ_{rr} peak. If this decrease in contact angle is ignored in the stress analyses, the corresponding predictions for CRB damage onset strength would be unconservative and equivalent to a horizontal bearing strength cutoff line in the bearing-bypass diagram.

Local Stress Superposition

Bearing-bypass stress analyses could be simplified if separate solutions for bearing and bypass loading could be superposed to obtain an approximate solution. This approach was used in [12] and is studied here by comparing results for simultaneous bearing and bypass loading from the present analysis with results based on superposition. To further simplify the approach, the bearing analysis was conducted for the linear c = 0 case as well as with the nonlinear c = 0.076mm case.

The stress distributions used in the superposition procedure are shown in figure 11. The dashed curve represents an all-bypass case with S_{np} = 250 MPa. The other three curves show different all-bearing cases with S_b = 250 MPa. The solid curve corresponds to TRB with a 0.076 mm clearance. The dash-dot curve represents the TRB case with c = 0. This special TRB case has a contact angle of about 82° which does not change with loading. This dash-dot curve represent a linear solution that can be scaled to represent other S_b loading levels. The dash-double-dot curve corresponds to the CRB case with c = 0, which is also linear and has a contact angle of about 78°.

The bearing (solid) curve with clearance and the bypass (dashed) curve in figure 11 were summed to get the dashed curve in figure 12. This dashed curve provides a reasonably good approximation to the $\sigma_{\theta\theta}$ solid curve, corresponding to simultaneous bearing-bypass (β = 1) loading. The dashed curve for σ_{rr} underestimates the contact angle by about 15°. Therefore, the σ_{rr} peak is overestimated by about 20 percent and occurs at θ = 0° rather than near 45°, as indicated by the solid curve. The dash-dot curve represents the superposition of the c = 0 bearing and the bypass case. This dash-dot curve also provides a good approximation for the $\sigma_{\theta\theta}$ distribution, but overestimates the contact angle by about 20°, resulting in a 10 percent error in the σ_{rr} peak value. In a NT critical case such as this [2], the σ_{rr} stresses are not important and either of these superposition approaches would provide accurate $\sigma_{\theta\theta}$ net-section (θ = 90°) stresses needed to predict NT damage onset.

A similar comparison for β = -1 is shown in figure 13. Again, the stresses for bypass loading can be superimposed on either the c = 0.076 mm bearing case or the c = 0 bearing case to estimate the net-section (θ = 90°) $\sigma_{\theta\theta}$ stresses needed to predict NC damage onset. However, in the present study, β = -1 loading was found to produce CRB damage as well as NC damage, so the σ_{rr} stresses are also important for this case. Neither of the superposition curves in figure 13 approximates σ_{rr} very well. The bearing case with c = 0.076 mm (dashed curve) overestimates the contact angle by about 15° and underestimates the σ_{rr} peak by almost 30 percent. The bearing case with c = 0 (dash-double-dot curve) overestimates contact by more than 40° and underestimates the σ_{rr} peak by almost 50 percent.

Although bearing-bypass superposition has been examined only for two specific cases in figures 12 and 13, these results suggest that superposition may provide useful estimates of the $\sigma_{\theta\theta}$ stresses associated with net-section damage in tension as well as compression. However, contact angle errors produce significant errors in the peak σ_{rr} values. As a result, superposition may lead to unacceptably large errors in bearing damage-onset predictions.

The superposition of stress results can also provide some insight into a load interaction for the NC damage mode that was not investigated in the present study.

Figure 11 shows that CRB loading produces tensile $\sigma_{\theta\theta}$ stress on the hole boundary at the net section (θ = 90°). Of course, compressive bypass loading produces compressive $\sigma_{\theta\theta}$ on the net section. As a result, in compressive bearing-bypass loading, the bearing loads tend to reduce the compressive $\sigma_{\theta\theta}$ stress that governs NC damage onset. Therefore, CRB loads should increase the NC damage-onset strength compared to the all-bearing bypass (β = -0) case. This is an area of bearing-bypass behavior that needs further research.

CONCLUDING REMARKS

A combined experimental and analytical study was conducted to investigate the effects of bolt-hole contact on bearing-bypass strength of a graphite/epoxy laminate. The T300/5208 specimens consisted of 16-plies with a quasi-isotropic layup and had a centrally located hole. Bearing loads were applied through a steel bolt having a clearance fit. Damage-onset strength and damage mode were determined for each test case. A 2-D finite element procedure was used to calculate hole-boundary stresses and bolt contact for each measured damage-onset strength.

For loading levels corresponding to damage onset, the cases of pure bearing in either tension or compression had bolt contact over a half-angle of only about 60°, compared to the 90° value often assumed in bearing stress analyses. For the tension bearing-bypass, the bolt contact angle at damage onset was approximately 60° for the whole range of bearing-bypass combinations investigated. In contrast, for compression, the contact angle decreased to about 35°.

In compression, the bearing damage-onset strengths showed an interaction of the bearing and bypass loads. Compressive bypass loads reduced the bearing damage-onset strength. This interaction was explained by the decrease in the bolt-hole contact angle that increased the severity of the bearing loads.

In addition to the simultaneous bearing and bypass loading, hole boundary stresses were also computed by superimposing stresses for separate bearing and bypass loading. A comparison of results showed that stresses at the specimen net section were accurately approximated by the superposition procedure. However, this procedure did not accurately calculate the peak bearing stresses because the bolt contact angles were not accurately represented. For compression bearing-bypass loading, the peak bearing stress errors of nearly 50 percent were calculated.

This study showed that bolt-hole contact had an influence on bearing damage-onset strength and must, therefore, be represented properly to obtain accurate stress analyses, especially for compression bearing-bypass loading.

REFERENCES

1. Hart-Smith, L. J.: "Bolted Joints in Graphite/Epoxy Composites". NASA CR-144899, National Aeronautics and Space Administration, January 1977.

2. Crews, J. H., Jr. and Naik, R. A.: "Combined Bearing and Bypass Loading on a Graphite/Epoxy Laminate". Composite Structures, Vol. 6, 1986, pp. 21-40.

3. Naik, R. A.: "An Analytical and Experimental Study of Clearance and Bearing-Bypass Load Effects in Composite Bolted Joints". Ph.D. dissertation, Old Dominion University, Norfolk, Virginia, August 1986.

4. Crews, J. H. ,Jr. and Naik, R. A.: "Bearing-Bypass Loading on Bolted Composite Joints". Presented at AGARD Symposium on Behavior and Analysis of Mechanically Fastened Joints in Composite Structures, AGARD-CP-427, Madrid, Spain, April 27-29, 1987. Also published as NASA TM-89153, May 1987.

5. Naik, R. A. and Crews, J. H., Jr.: "Stress Analysis Method for Clearance-Fit Joints with Bearing-Bypass Loads". Presented at AIAA/ASME/ASCE/AHS 30th Structures, Dynamics, and Materials Conference, April 3-5,1989, Mobile, Alabama, 1989 (AIAA Paper 89-1230), Also published as NASA TM-100551, Jan. 1989.

6. Naik, R. A. and Crews, J. H., Jr.: "Ply-Level Failure Analysis of a Graphite/Epoxy Laminate under Bearing-Bypass Loading". NASA TM-100578, March 1988.

7. Mangalgiri, P. D., Dattaguru, B., and Rao, A. K.: "Finite Element Analysis of Moving Contact in Mechanically Fastened Joints". Nuclear Engineering Design, Vol. 78, 1984, pp. 303-311.

8. Naik, R. A. and Crews, J. H. Jr.: "Stress Analysis Method for a Clearance-Fit Bolt under Bearing Loads". AIAA Journal Vol. 24, No. 8, August 1986, pp. 1348-1353.

9. Crews, J. H., Jr., Hong, C. S., and Raju, I. S.: "Stress-Concentration Factors for Finite Orthotropic Laminates with a Pin-Loaded Hole". NASA TP 1862, May 1981.

10. Soni, S. R.: "Failure Analysis of Composite Laminates with a Fastener Hole". AFWAL-TR-80-4010, March 1980.

11. Ramkumar, R. L.: "Bolted Joint Design". Test Methods and Design Allowables for Fiberous Composites. ASTM STP 734, C. C. Chamis, Ed., American Society for Testing and Materials, 1981, pp.376-395.

12. Garbo, S. P. and Ogonowski, J. M.: "Effect of Variances and Manufacturing Tolerances on the Design Strength and Life of Mechanically Fastened Composite Joints". Methodology Development and Data Evaluation, AFWAL-TR-81-3041, I-III, April 1981.

Table 1. Damage-onset test data.

	β	S_g (MPa)	S_b (MPa)	S_{np} (MPa)	θ_1 (deg)	Failure mode
Tension	0	265	0	304	--	NT
	1	237	237	237	60.9	NT
	3	196	468	156	62.8	NT
	∞	69.5	542	0	60.0	TRB
Compression	0	-368	0	442	--	NC
	-1	-324	324	-324	34.7	CRB/NC
	-3	-209	498	-166	47.8	CRB
	$-\infty$	-67.7	528	0	56.2	CRB
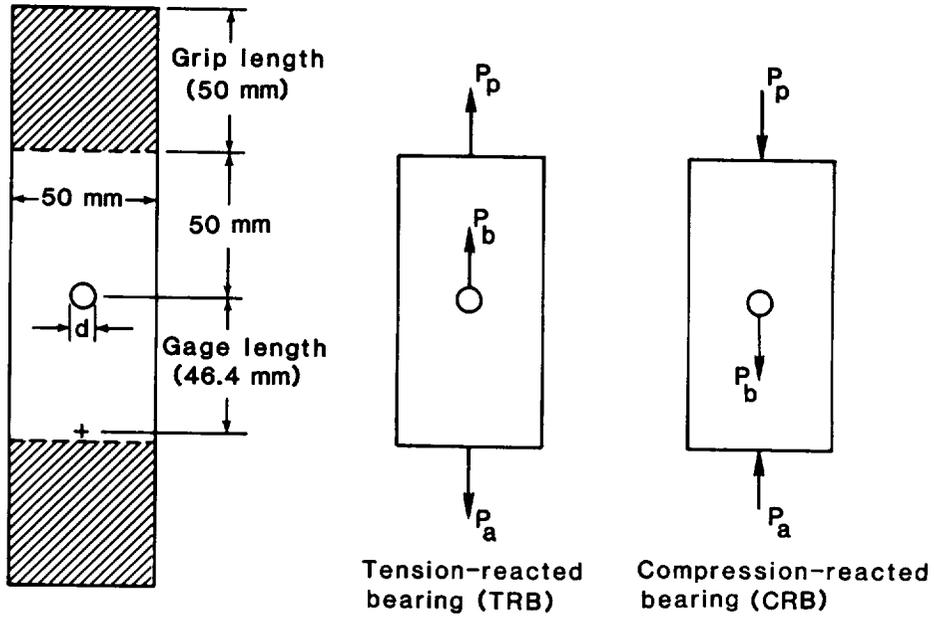
(a) Test specimen

(b) Bearing-bypass loading

Figure 1. Specimen configuration and bearing-bypass loading.
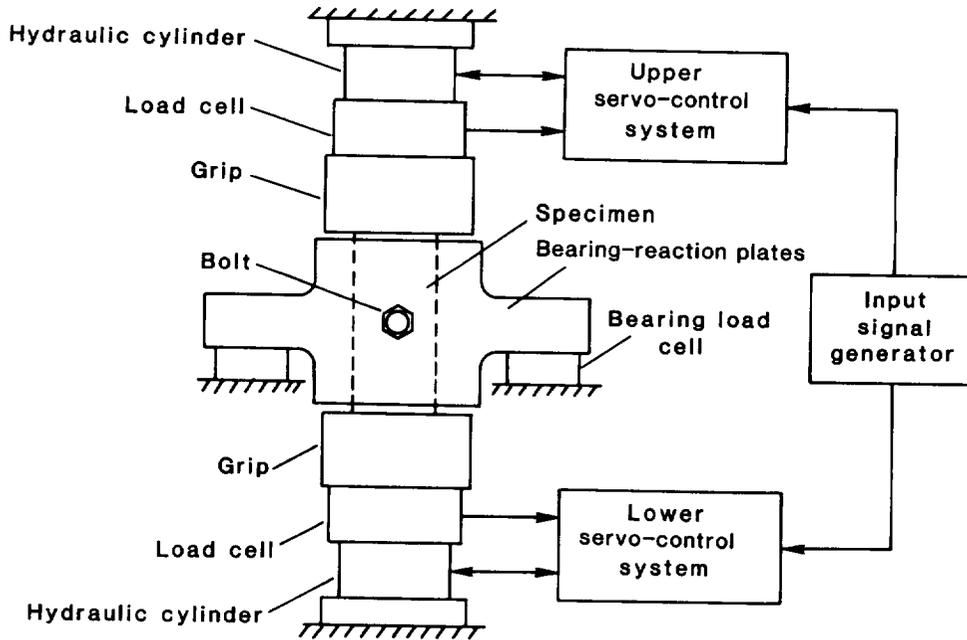
Figure 2. Schematic of the bearing-bypass test system.

(a) Net-section tension (NT)

(b) Tension-reacted bearing (TRB)

(c) Compression-reacted bearing (CRB)

(d) Net-section compression (NC)
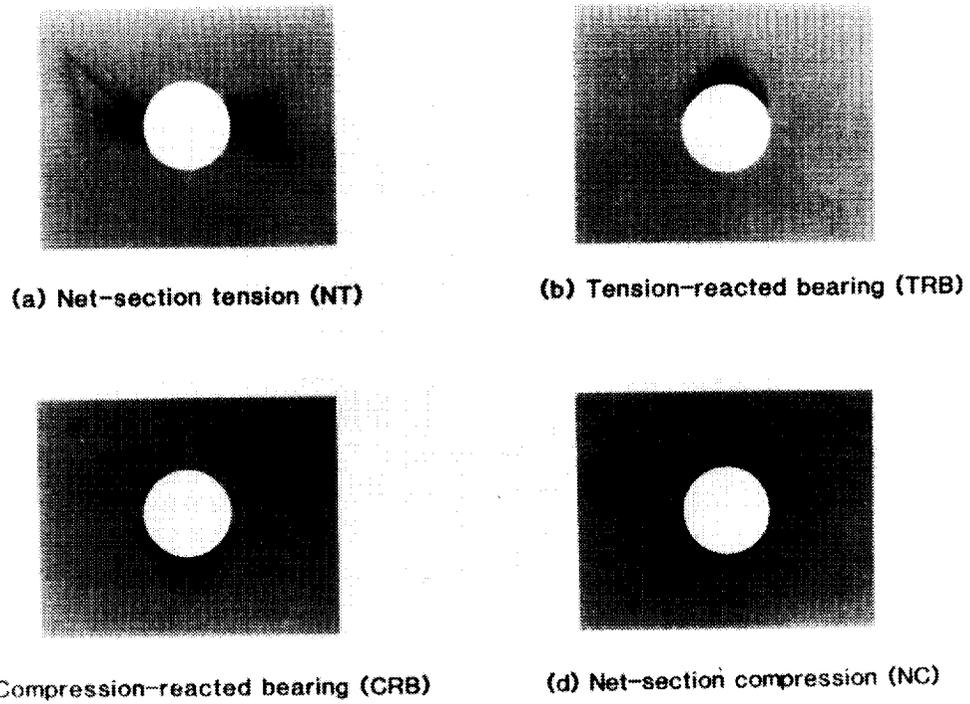
Figure 3. Radiographs of damage at fastener hole.
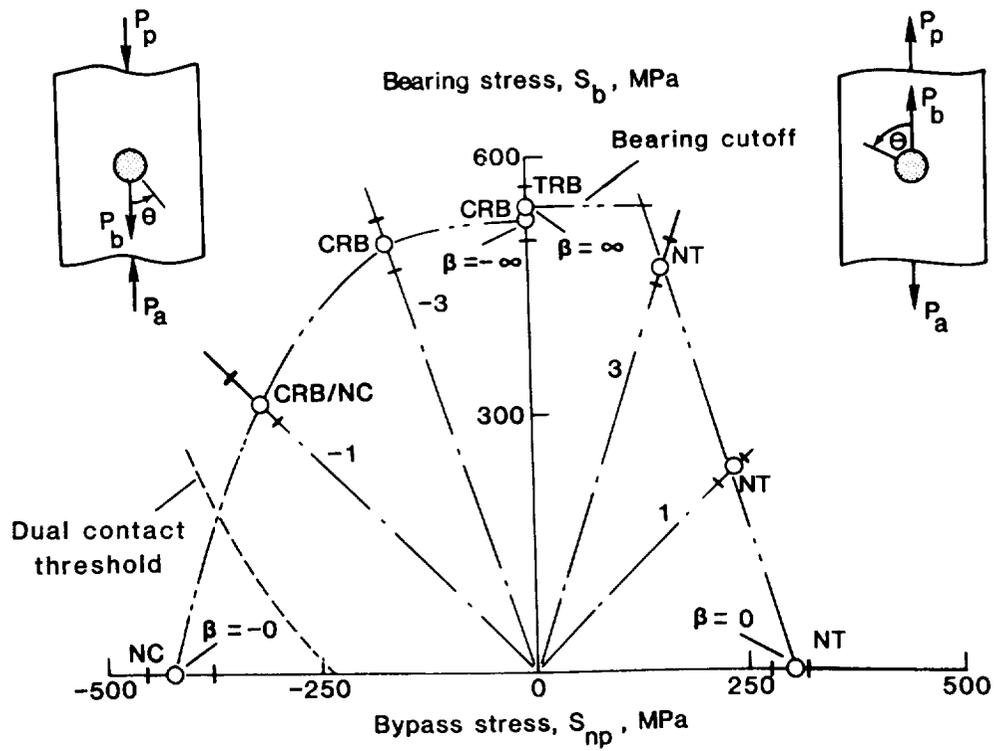
Figure 4. Bearing-bypass diagram for damage-onset strength.

932
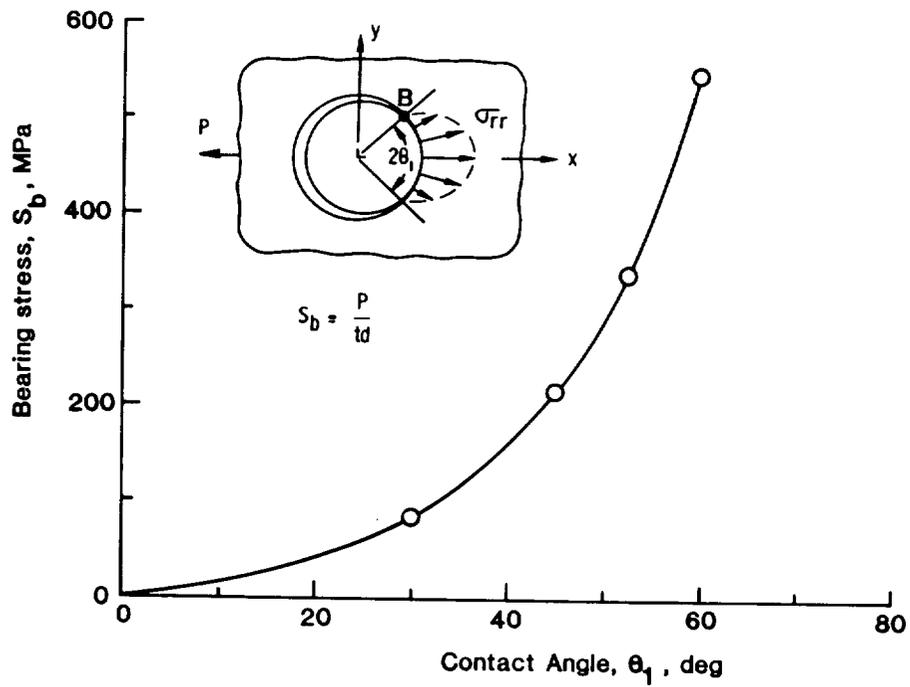
Figure 5. Nonlinear relationship between bearing stress and contact angle.

(a) Single contact.   (b) Dual contact.
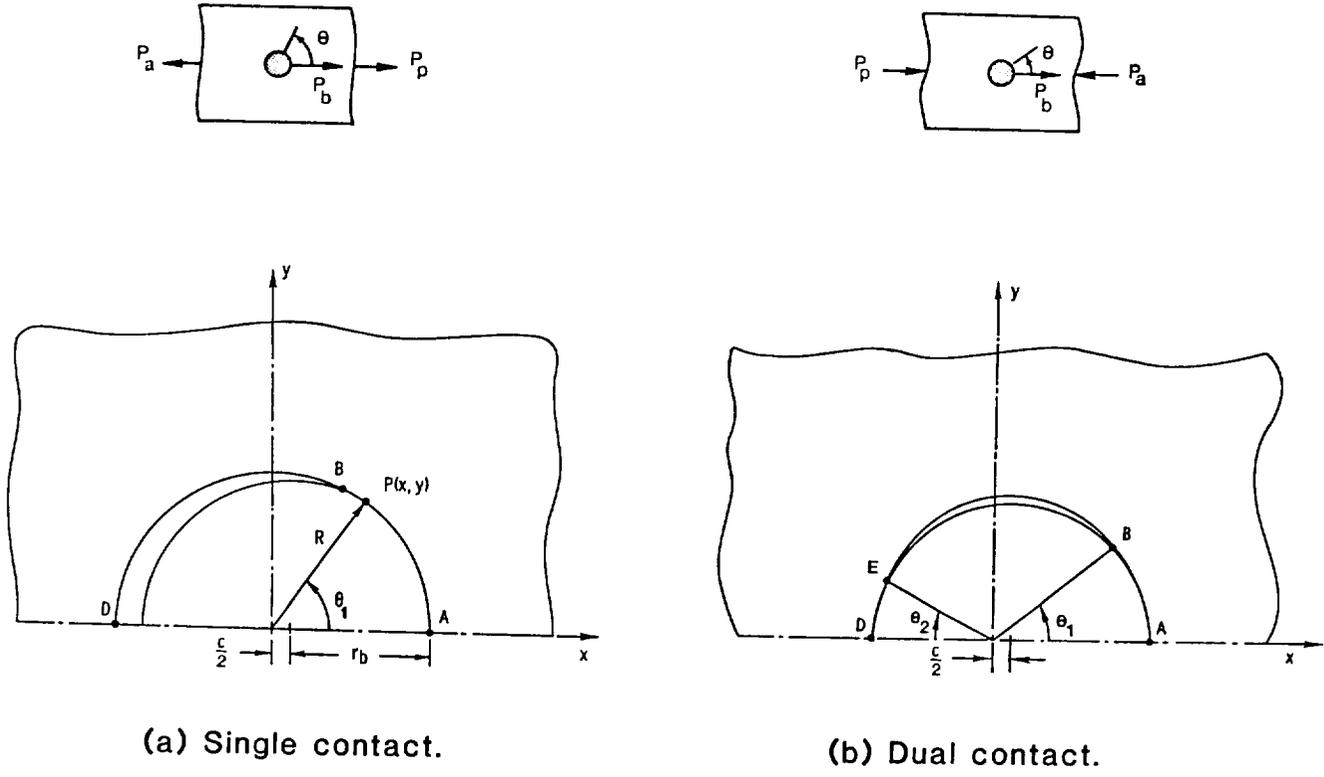
Figure 6. Bolt-hole contact under bearing-bypass loading.

β	S_b (MPa)	S_{np} (MPa)	Damage mode
0	0	304	NT
1	237	237	NT
3	468	156	NT
∞	542	0	TRB
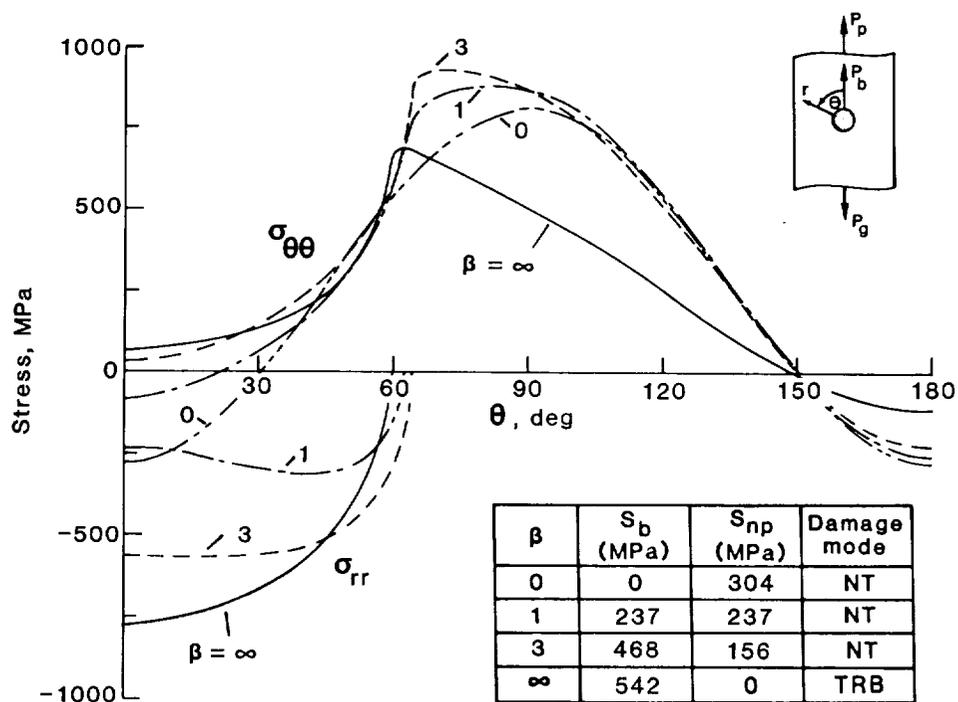
Figure 7. Stress distributions for tension bearing-bypass loading.

β	S_b (MPa)	S_{np} (MPa)	Damage mode
-0	0	-422	NC
-1	-324	-324	CRB/NC
-3	498	-166	CRB
-∞	528	0	CRB
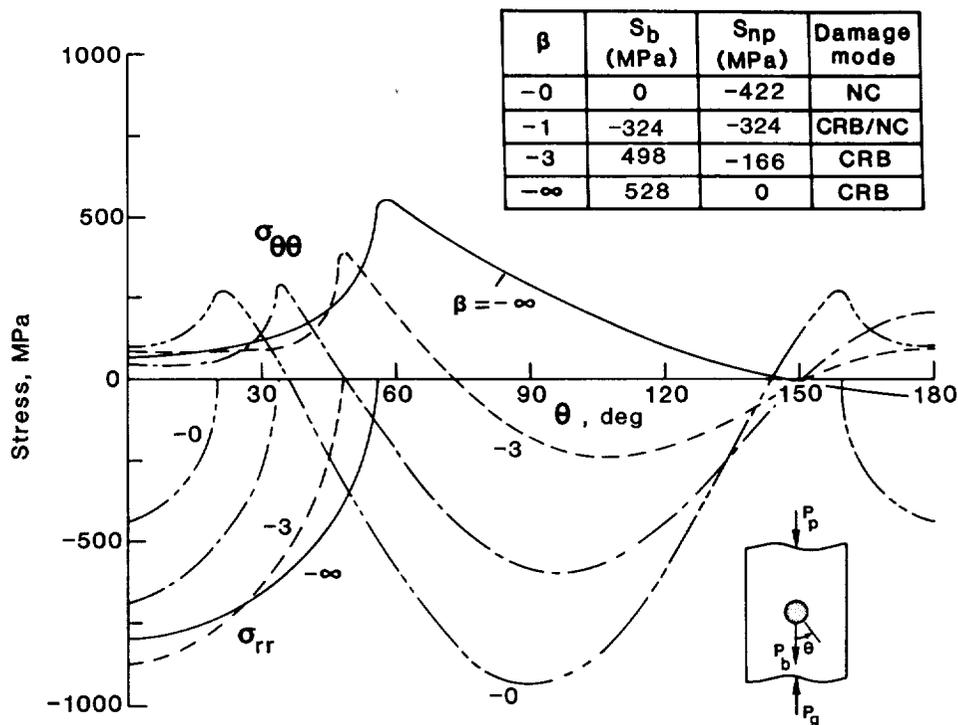
Figure 8. Stress distributions for compression bearing-bypass loading.

934
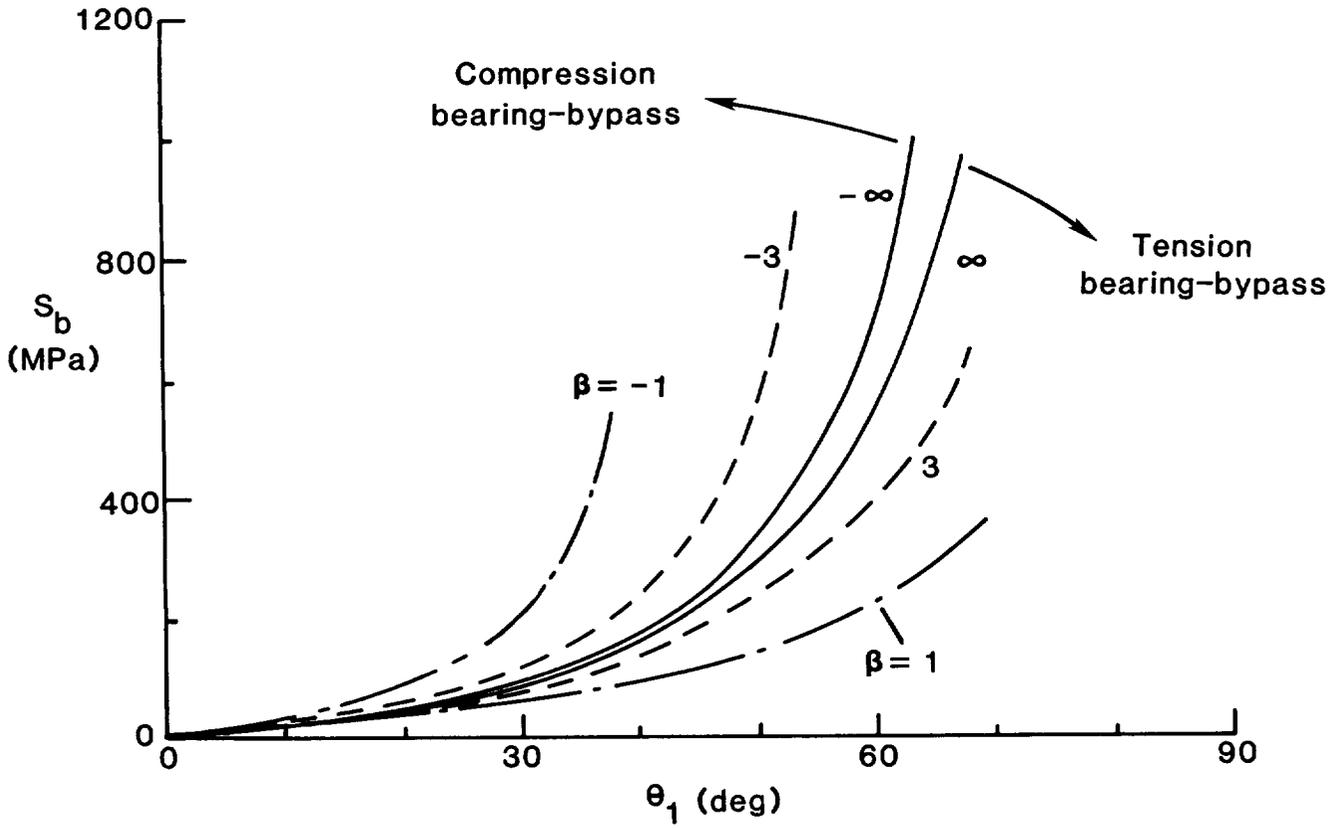
Figure 9. Variation of bolt-hole contact angle with bearing loading.
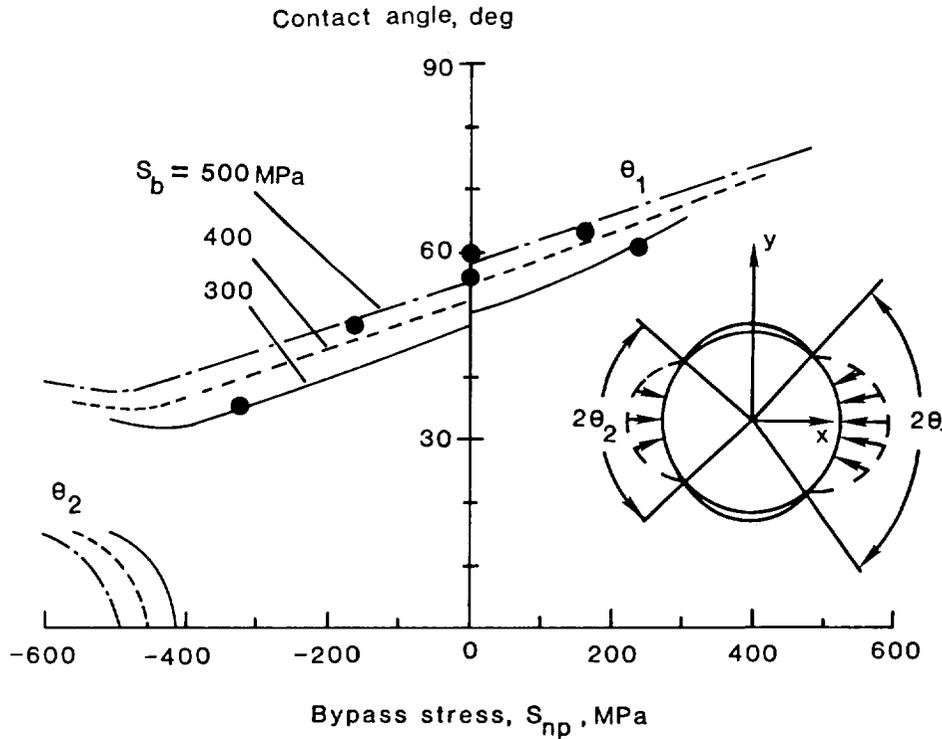
Figure 10. Variation of bolt-hole contact angle with bypass loading.
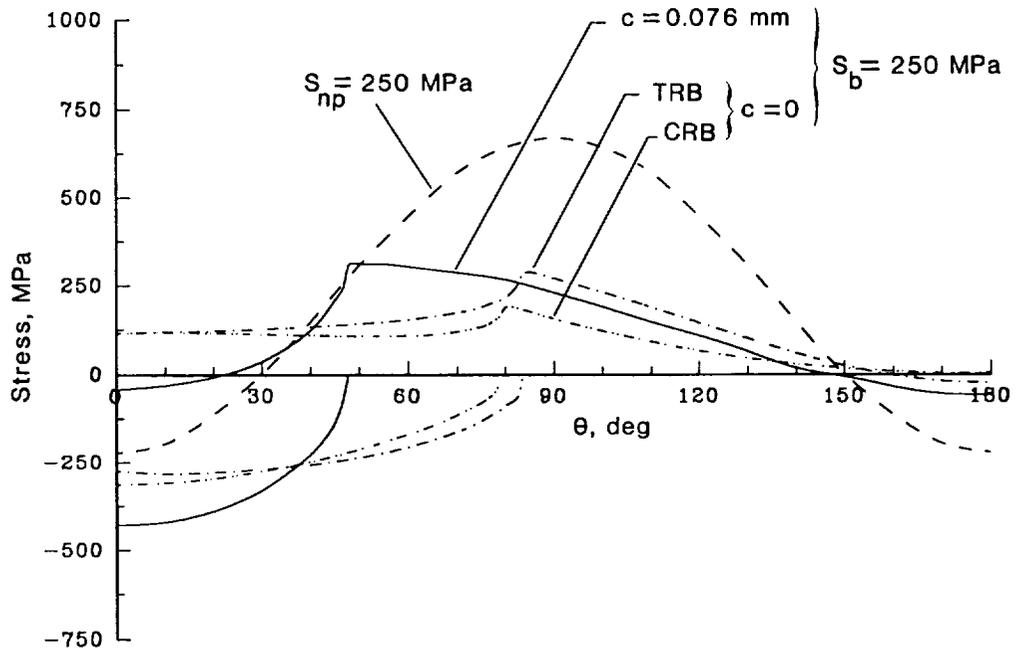
Figure 11. Stress distributions for bypass loading and bearing loading.
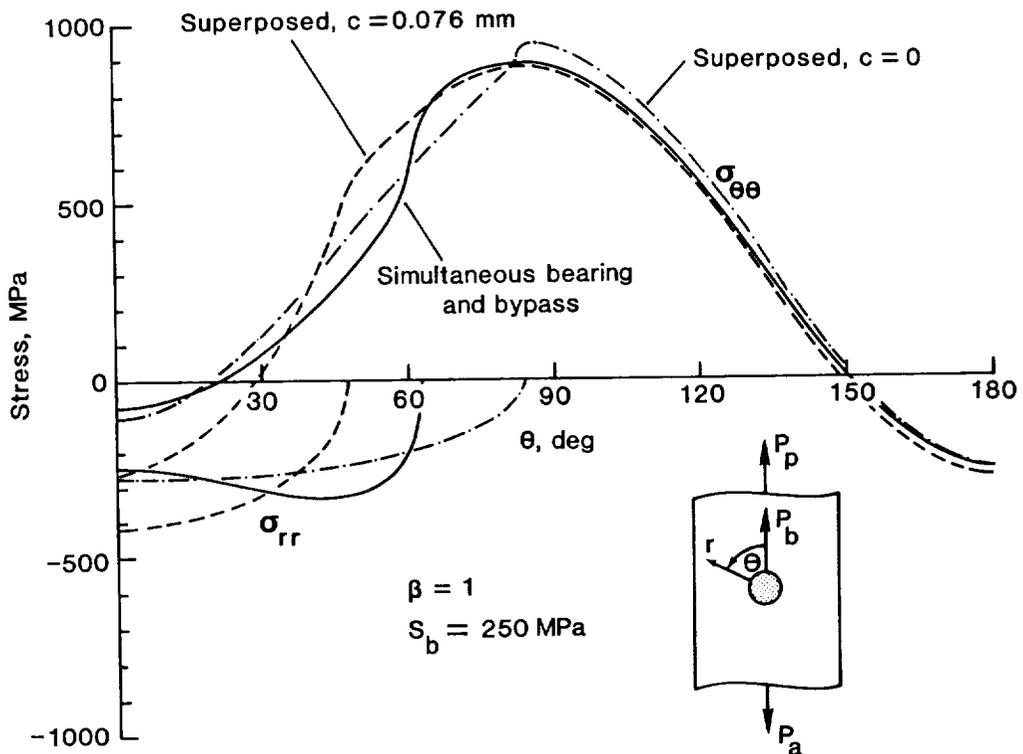
Figure 12. Superposition of tension-reacted bearing and tension bypass stresses.

936
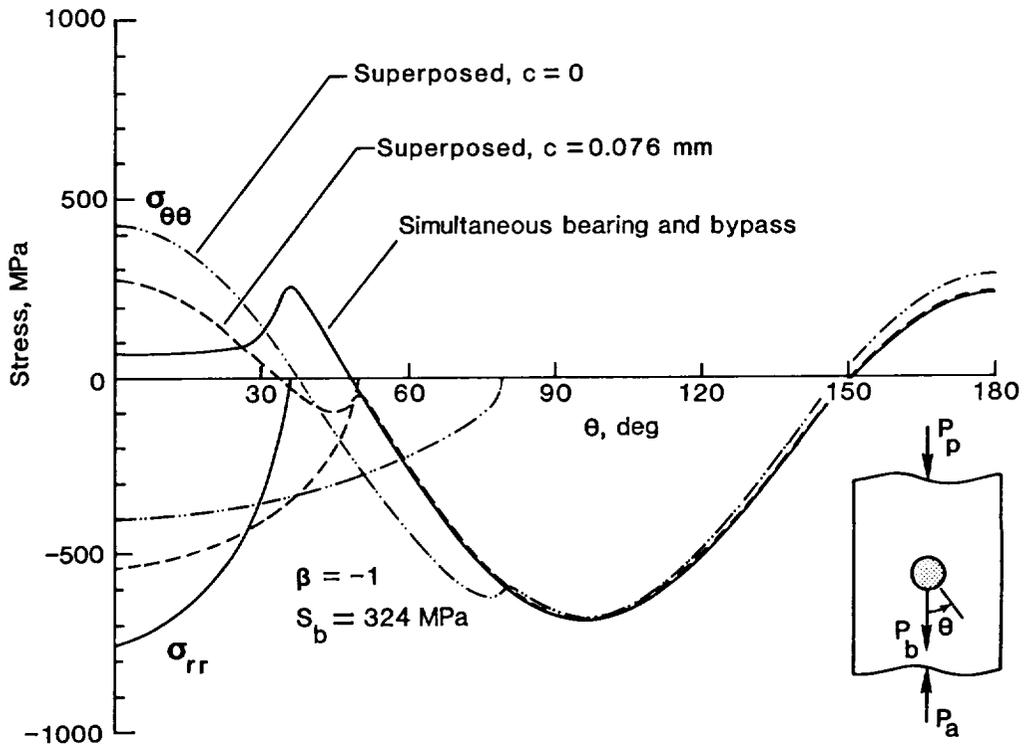
Figure 13. Superposition of compression-reacted bearing and compression
bypass stresses.